

Nodes Are Early, Edges Are Late: Probing Diagram Representations in Large Vision-Language Models

Haruto Yoshida¹, Keito Kudo¹, Yoichi Aoki¹, Ryota Tanaka²,
Itsumi Saito¹, Keisuke Sakaguchi¹, Kentaro Inui¹,

¹Tohoku University, ²Human Informatics Labs., NTT, Inc.

{yoshida.haruto.p1, keito.kudo.q4, youichi.aoki.p2}@dc.tohoku.ac.jp,
ryota.tanaka@ntt.com, {itsumi.saito, keisuke.sakaguchi}@tohoku.ac.jp,
kentaro.inui@mbzuai.ac.ae

Abstract

Large vision-language models (LVLMs) demonstrate strong performance on diagram understanding benchmarks, yet they still struggle with understanding *relationships* between elements, particularly those represented by nodes and directed edges (e.g., arrows and lines). To investigate the underlying causes of this limitation, we probe the internal representation of LVLMs using a carefully constructed synthetic diagram dataset based on directed graphs. Our probing experiments reveal that edge information is not linearly separable in the vision encoder and becomes linearly encoded only in the text tokens in the language model. In contrast, node information and global structural features are already linearly encoded in individual hidden states of the vision encoder. These findings suggest that the stage at which linearly separable representations are formed varies depending on the type of visual information. In particular, the delayed emergence of edge representations may help explain why LVLMs struggle with relational understanding, such as interpreting edge directions, which require more abstract, compositionally integrated processes.

1 Introduction

Diagrams convey complex information through visual layouts that people can grasp quickly, making them an important communication medium across various domains, including academic research (Hsu et al., 2021; Kohn and Aladjem, 2006) and business (Jošt et al., 2017; Kernbach and Eppler, 2010). To support clearer communication with diagrams, many systems for diagram understanding have been studied (Kembhavi et al., 2016; Li et al., 2025).

Large vision-language models (LVLMs) (Bai et al., 2025a,b; Liu et al., 2024; Team et al., 2025) have shown strong performance on benchmark tasks related to diagram understanding (Zhang et al., 2025; Lu et al., 2024). However, prior stud-

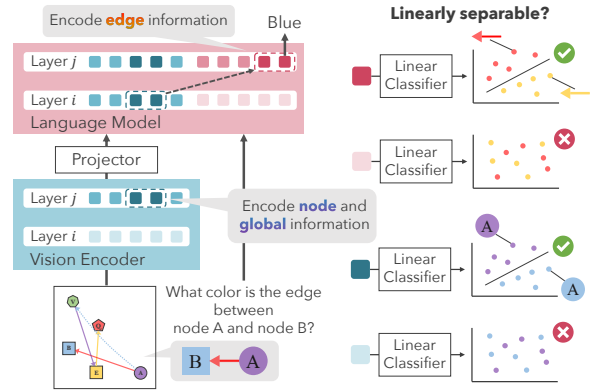


Figure 1: Overview of this study. We analyze internal representations in LVLMs using probing on a synthetic diagram dataset. We find that node information (e.g., node color) and global information (e.g., node count) are linearly encoded in a single image patch within the vision encoder, whereas edge information (e.g., edge color) is linearly encoded in a single text token within the language model.

ies report that LVLMs still struggle with understanding certain visual elements in diagrams, such as relational information indicated by arrows and lines (Hou et al., 2025; Zhu et al., 2025; Pan et al., 2024). Understanding the causes of these limitations requires analyzing how LVLMs internally represent visual elements in diagrams, yet no prior work has comprehensively examined this for the basic elements such as nodes, edges, and global structure.

To fill this gap, we comprehensively investigate how diagram-specific visual elements are internally distinguished in LVLMs. We focus on where and when information about nodes, edges, and global structure becomes accessible within the vision encoder and the language model. In contrast to prior analyses that focus on natural images (Gandelsman et al., 2024; Tao et al., 2024), our work targets diagrams, which rely on symbolic representations to express structured relationships. To enable con-

Category	Aspect a	Label set \mathcal{Y}
Single	Node Color	{red, green, yellow, blue, brown, orange, pink, purple}
	Node Shape	{circle, square, pentagon, hexagon, septagon}
	In-degree	{0, 1, 2, 3, 4}
	Out-degree	{0, 1, 2, 3, 4}
Multiple	Edge Color	{red, green, yellow, blue, brown, orange, pink, purple}
	Edge Style	{solid, dashed}
	Edge Existence	{exist, not exist}
	Edge Direction	{forward, backward}
	Multi-hop Path	{exist, not exist}
Global	Node Count	{1, 2, 3, 4, 5}
	Edge Count	{1, 2, 3, 4, 5}

Table 1: The 3 categories, 11 aspects, and their corresponding label sets \mathcal{Y} .

trolled analysis, we construct a synthetic diagram dataset as a testbed and apply probing (Alain and Bengio, 2017) and causal intervention (Zhang and Nanda, 2024) methods to examine the linear separability of node, edge, and global information within the vision encoder and the language model. Linear separability is commonly used as an indicator of whether information is explicitly encoded and readily accessible to the model.

Our contributions are threefold. First, we introduce a synthetic diagram dataset with controllable visual elements, enabling controlled analysis while reducing the influence of domain-specific knowledge. Second, our probing analysis shows that node and global information are already linearly encoded in a single image patch in the vision encoder, whereas edge information becomes linearly encoded in a single text token in the language model. This difference correlates with the model’s weaker performance on edge-related tasks. Third, through causal interventions, we verify that visual information linearly encoded in the vision encoder, such as node attributes and the number of nodes, has a causal effect on the model’s final predictions. These findings clarify how visual information is internally represented in LVLMs and offer guidance for the design and analysis of future diagram understanding systems.¹

2 Task and Model Setup

As a testbed for our analysis, we evaluate the VQA task on synthetically created simple diagram images (graphs). This VQA task can be solved as

¹The code and data will be released upon acceptance.

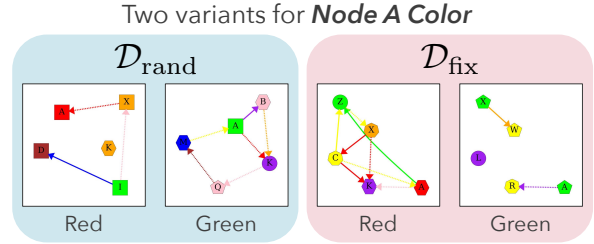


Figure 2: Examples of synthetic diagrams. Each diagram contains five nodes, and we control evaluation aspects such as node color, shape, and edge connectivity. We provide two variants: $\mathcal{D}_{\text{rand}}$, which uses random node layouts (left part), and \mathcal{D}_{fix} , which uses fixed layouts (right part).

a classification task. As shown in Figure 1, the LVLm takes as input a synthetically created simple diagram image x and a question q , and outputs the answer $y \in \mathcal{Y}$ (where \mathcal{Y} is the set of answer labels) to the question as text.

In our experiments, we primarily focus on Qwen3-VL-8B-Instruct (Bai et al., 2025a) as the main target of analysis. In addition, we conduct the same experiments on Qwen2.5-VL 7B (Bai et al., 2025b), LLaVA1.5 7B (Liu et al., 2024), and Gemma3-4B-IT (Team et al., 2025). These results are reported in Appendix C and D.

3 Dataset

To investigate how LVLms perceive basic visual elements in diagrams, we construct a synthetic diagram dataset. This dataset consists of synthetic diagrams generated from directed graphs with nodes and edges. This setup allows us to precisely control evaluation factors such as node color and edge direction. Moreover, using synthetic data helps reduce biases and shortcuts inherited from natural-image and natural-language datasets (Kafle and Kanan, 2017; Gururangan et al., 2018; Dancette et al., 2021; Healey et al., 2024). As a result, we can conduct fine-grained analysis and evaluation.

3.1 Diagram Specification

Each diagram satisfies the following properties: (1) Nodes and edges are colored using one of eight colors: red, green, yellow, blue, brown, orange, pink, or purple. (2) Each diagram contains 5 nodes. (3) Node shapes are one of circle, square, pentagon, hexagon, or septagon. (4) Each node is labeled with a single alphabetic character as an identifier. (5) Edge styles are either solid or dashed. Further details are provided in Appendix B.1.

3.2 Evaluation Aspects

We define 11 aspects as basic visual information in diagrams, as shown in Table 1. These aspects are based on visual information emphasized in prior works (Silva et al., 2011; Pan et al., 2024; Sterzik et al., 2024; Tseng et al., 2025; Hou et al., 2025; Zhu et al., 2025). Moreover, these aspects are classified into the following three categories:

- **Single:** Visual information localized around a single node.
- **Multiple:** Combinations of multiple localized pieces of visual information. Since edges are defined between two nodes, their recognition requires a multi-step process: first identifying the endpoint nodes, then recognizing the edge attributes between them.
- **Global:** Visual information that cannot be determined without considering all nodes and edges in the diagram.

In analyzing each aspect, we focus on attributes of the node with identifier A (node A) and the edge connecting nodes A and B (edge AB) as representatives². For example, in the ‘‘Node Color’’ aspect, we evaluate whether the color of node A is represented (i.e., linearly decodable) in the model.

3.3 Dataset Definition

For each aspect a , we define a dataset \mathcal{D} to verify whether it can be recognized as follows:

$$\mathcal{D} = \{(x_i, y_i)\}_{i=1}^N. \quad (1)$$

Here, x_i is the i -th diagram image and y_i is its label. Specifically, this is a dataset containing labels y_i for each aspect as shown in Table 1.

In this study, we train probes to analyze the internal representations of an LVLM. To train and evaluate these probes, for each aspect, we construct two variants with different node layouts:

- $\mathcal{D}_{\text{rand}}$: For each diagram in the dataset, the node layout is determined independently at random.
- \mathcal{D}_{fix} : For all diagrams in the dataset, nodes with each identifier are placed at the same spatial position.

²The choice of identifiers is arbitrary, and similar experiments can be conducted focusing on other identifiers such as node C, but we select A and B as representatives here.

Figure 2 shows examples of each variant. For each aspect, both $\mathcal{D}_{\text{rand}}$ and \mathcal{D}_{fix} consist of 100 data points per classification class. That is, the size of each variant is $|\mathcal{Y}| \times 100$.

Training dataset for probing. We construct the diagram dataset with random node layouts, $\mathcal{D}_{\text{train}}$, as the base for the probe training dataset. In pilot experiments, we observed that the probe achieved near-perfect accuracy on certain patches by exploiting shortcuts, such as predicting based on colors present in the input patch without identifying the target node or edge (see Appendix C.1 for details). To prevent this, we prepare an additional dataset $\mathcal{D}_{\text{rand}}^\perp$, which consists of diagrams in which the target node or edge does not exist, with the gold label $y = \perp$ (e.g., the question asks about node A, but node A does not exist in the image). This forces the probe to verify target existence before predicting its attributes, which resolved the shortcut issue in our experiments. $\mathcal{D}_{\text{rand}}^\perp$ contains the same number of samples as $\mathcal{D}_{\text{rand}}$. Using $\mathcal{D}_{\text{rand}}^\perp$, we define the probe training dataset as $\mathcal{D}_{\text{train}} = \mathcal{D}_{\text{rand}} \cup \mathcal{D}_{\text{rand}}^\perp$.

Evaluation dataset for probing. We prepare the evaluation dataset by constructing M variants of \mathcal{D}_{fix} . Formally, denoting the j -th evaluation subset as $\mathcal{D}_{\text{fix}}^j$, the entire evaluation dataset is expressed as $\mathcal{D}_{\text{test}} = \{\mathcal{D}_{\text{fix}}^0, \mathcal{D}_{\text{fix}}^1, \dots, \mathcal{D}_{\text{fix}}^{M-1}\}$.

This evaluation dataset has the following advantages:

- The fixed node layout allows us to analyze the model’s internal representations in a controlled manner.
- Evaluating across M variants of \mathcal{D}_{fix} enables us to verify that the observed behaviors are not artifacts arising from a specific spatial configuration.

4 Preliminary: VQA

We evaluate the VQA performance of LVLMs on synthetic diagrams as a preliminary experiment to confirm that the models achieve above-chance-level performance through meaningful inference rather than random guessing. Specifically, we assess whether the models can correctly predict the gold label y given a diagram x and question q in a simple VQA setting. The question q includes the label set \mathcal{Y} as answer choices. For example, for the Node Color aspect, the question is ‘‘What color is

	Node Color	Node Shape	In-degree Count	Out-degree Count	Edge Color	Edge Style	Edge Existence	Edge Direction	Multi-hop Path	Node Count	Edge Count
Chance level	12.5	20.0	20.0	20.0	12.5	50.0	50.0	50.0	50.0	20.0	20.0
Qwen3-VL 8B	91.4	76.6	40.3	34.7	57.3	73.5	69.6	49.3	58.3	40.3	21.6

Table 2: Acc_{VQA} for Qwen3-VL 8B. Accuracy exceeded chance level for all aspects except Edge Direction.

node A?” with choices $\mathcal{Y} = \{\text{red, green, } \dots\}$. The same input format is used in the probing and causal intervention experiments. The full list of questions for each aspect is provided in Table 4.

4.1 Evaluation Metric

We define the final score as the mean accuracy across all evaluation data subsets. Formally, it is defined as:

$$\text{Acc}_{\text{VQA}}(q, \mathcal{D}_{\text{test}}) = \text{mean}_{d_{\text{fix}} \in \mathcal{D}_{\text{test}}} \text{acc}_{\text{VQA}}(q, d_{\text{fix}}). \quad (2)$$

Here, acc_{VQA} is the accuracy of the LVLM on the VQA task for dataset $d_{\text{fix}} \in \mathcal{D}_{\text{test}}$, and $\text{mean}_{s \in \mathcal{S}}(\cdot)$ denotes the element-wise arithmetic mean of the values associated with each $s \in \mathcal{S}$. We judge a prediction as correct if the LVLM’s output text contains the label y as a substring.

4.2 Experimental Results

Table 2 summarizes the Acc_{VQA} of Qwen3-VL 8B. The model performs above chance level on all aspects except edge direction, for which accuracy stays near chance. This suggests that Qwen3-VL captures most aspects but fails to reliably identify edge direction.

5 Probing

We aim to identify in which layers and at which image patches or tokens diagram visual information is represented (i.e., linearly decodable) within the LVLMs. To this end, we train probes at each layer of the vision encoder and language model, and evaluate the prediction performance of VQA answers from hidden states. Probing is an effective method for revealing at which stages of a model information is progressively encoded (Alain and Bengio, 2017). It is generally assumed that if specific information is encoded in a linearly separable form, the model can readily access that information (Hewitt and Liang, 2019).

5.1 Probe Definition

Let $\mathbf{h}_{l,t}$ denote the hidden state at layer l and position t of the vision encoder or language model

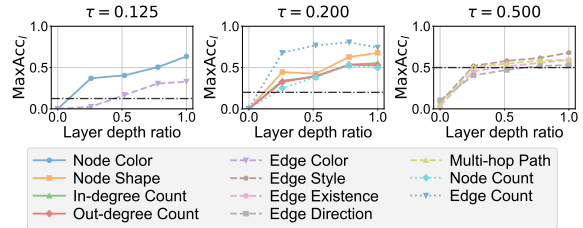


Figure 3: Layer-wise maximum accuracy in the vision encoder of Qwen3-VL 8B. The x-axis denotes the relative layer position (0 is the input layer and 1 is the final layer), and the y-axis denotes accuracy. Aspects sharing the same threshold are drawn with the same line style, which also matches the style of the corresponding black threshold lines.

when inputting diagram x and question text q . The probe f that predicts the VQA task answer or \perp from the hidden state is defined as a single-layer linear classifier:

$$\hat{y} = f(\mathbf{h}_{l,t}) = \arg \max_{\mathcal{Y} \cup \{\perp\}} \mathbf{W} \mathbf{h}_{l,t} + \mathbf{b}, \quad (3)$$

where $\hat{y} \in \mathcal{Y} \cup \{\perp\}$ denotes the predicted answer label, $\mathbf{W} \in \mathbb{R}^{(|\mathcal{Y}|+1) \times |\mathbf{h}_{l,t}|}$ is the weight matrix and $\mathbf{b} \in \mathbb{R}^{(|\mathcal{Y}|+1)}$ is the bias term.

We train probes and conduct probing separately for the following three components using the training dataset $\mathcal{D}_{\text{train}}$ described in § 3.3:

Vision encoder. We predict label y from the hidden state $\mathbf{h}_{l,t}$ corresponding to the image patch at position t . For training, we use hidden states at all positions t in layer l to train a probe f_l for each layer l .

Language model (image input part). Similar to the vision encoder probe, we train a probe f_l to predict label y from the hidden state $\mathbf{h}_{l,t}$ corresponding to the image patch at position t .

Language model (text input part). We predict label y from the hidden state $\mathbf{h}_{l,t}$ corresponding to the text token at position t . We train a probe $f_{l,t}$ independently for each hidden state at layer l and position t . The target positions t for the probe are all token positions in question q .

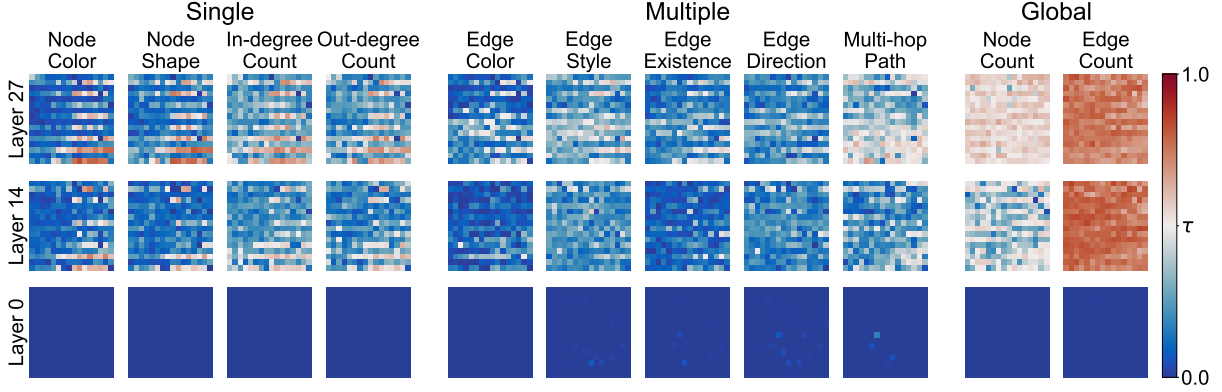


Figure 4: Position-wise accuracy in the vision encoder of Qwen3-VL 8B. Each heatmap shows accuracy by patch position for a specific layer and aspect. The node layout of the evaluation diagrams is the same as that of the diagrams in the right part of Figure 2.

5.2 Evaluation Metric

Let $acc_{l,t}(d_{\text{fix}})$ denote the accuracy of probe f (the match rate between \hat{y} and y) when using the hidden state at layer l and position t on evaluation data subset $d_{\text{fix}} \in \mathcal{D}_{\text{test}}$. The final evaluation score is the mean accuracy across all subsets:

$$Acc_{l,t}(\mathcal{D}_{\text{test}}) = \text{mean}_{d_{\text{fix}} \in \mathcal{D}_{\text{test}}} acc_{l,t}(d_{\text{fix}}). \quad (4)$$

In addition, as a measure of how well layer l represents (i.e., linearly decodes) the target visual information, we define the maximum probing accuracy at layer l , denoted as MaxAcc_l , as follows:

$$\text{MaxAcc}_l(\mathcal{D}_{\text{test}}) = \text{mean}_{d_{\text{fix}} \in \mathcal{D}_{\text{test}}} (\max_t acc_{l,t}(d_{\text{fix}})). \quad (5)$$

This MaxAcc_l computes, for each subset d , the maximum probing accuracy $acc_{l,t}(d)$ at layer l , and then averages it over all subsets in $\mathcal{D}_{\text{test}}$.

To assess whether probing is successful, we introduce a threshold $\tau = 1/|\mathcal{Y}|$ (the chance-level accuracy when excluding \perp). If $Acc_{l,t}$ exceeds this threshold τ , we conclude that probing is successful.

5.3 Experimental Results

Single and Global categories become linearly decodable in deeper layers, while Multiple remains difficult. Figure 3 reports MaxAcc_l at each layer of the vision encoder. For aspects in the Single and Global categories, accuracy increases gradually with depth, suggesting that deeper layers form representations that are increasingly linearly separable for these aspects. In contrast, accuracies for aspects in the Multiple category remain relatively low compared to the other categories even in the final layers, suggesting that these aspects are more

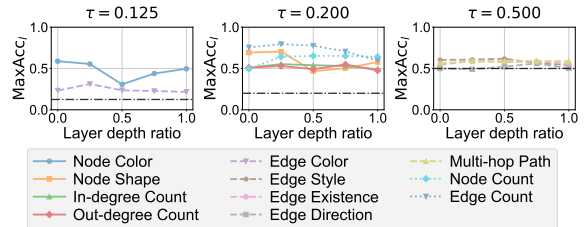


Figure 5: MaxAcc_l per layer in the language model of Qwen3-VL 8B. The x-axis denotes the layer position (0 is the input layer and 1 is the final layer), and the y-axis denotes accuracy. Aspects sharing the same threshold are drawn with the same line style, which also matches the style of the corresponding black threshold lines.

difficult to decode linearly from any single hidden state.

Single information is encoded near node positions, while Global information is encoded broadly across background regions. Figure 4 visualizes $acc_{l,t}(d_{\text{fix}})$ as heatmaps over layers and positions. In this figure, we report results using the same subset d_{fix} as the examples shown in the right part of Figure 2 (i.e., a dataset consisting of diagrams with the same node layout). For aspects in the Single category, high-accuracy patches are localized around the bottom-right area where the target node A is located, indicating that node information is encoded primarily in that region and nearby positions. For aspects in the Global category, accuracy rises above the threshold across almost all positions in later layers, suggesting that global information is distributed over a wide range of hidden states, including background regions. This high accuracy on background patches suggests that the vision encoder uses hidden states corresponding

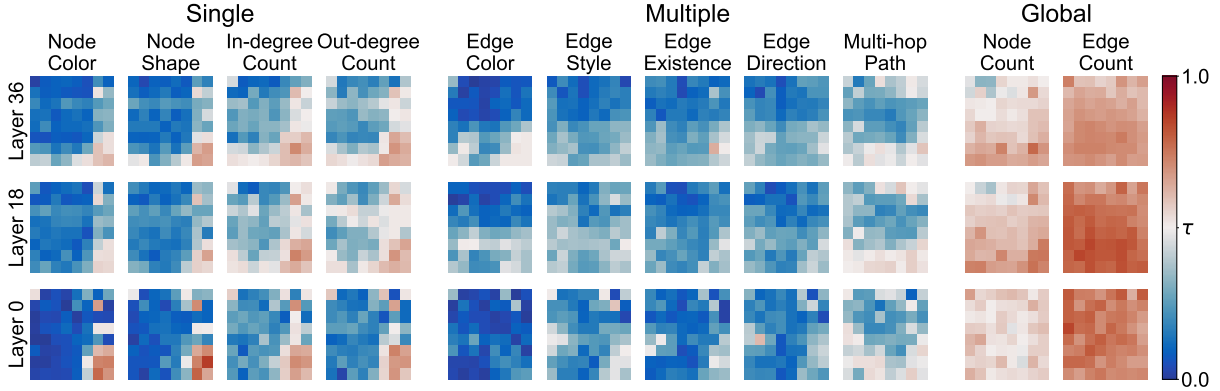


Figure 6: $acc_{l,t}(d_{\text{fix}})$ in the language model of Qwen3-VL 8B for a representative subset d_{fix} . The node layout of the evaluation diagrams is the same as that of the diagrams in the right part of Figure 2.

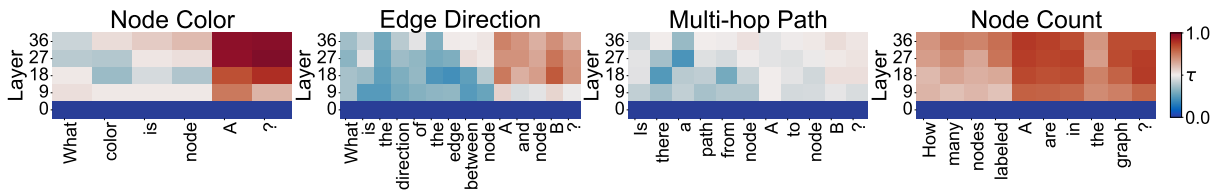


Figure 7: Probing results for text tokens in the language model of Qwen3-VL 8B. The x-axis shows token position in the question, and the y-axis shows layer position.

to background positions as storage or aggregation points for retaining and integrating visual information. While prior work on register tokens (Darcet et al., 2024) in Vision Transformer (Dosovitskiy et al., 2021) reports that global information is concentrated in a small subset (around 2%) of background tokens, our results suggest that global information is distributed across nearly all background patches in the diagram domain.

Limited changes in visual-information representations within the language model (image-input part). Figure 5 shows MaxAcc_l at each layer of the language model. MaxAcc_l at layer 0 showed no substantial change compared to the last layer of the vision encoder, suggesting that the information encoded by the vision encoder is almost preserved after passing through the adapter. However, MaxAcc_l for node color and shape slightly decreased from the middle layers onward, and aspects in the Multiple category dropped to around the threshold at the final layer, suggesting that information about these aspects may be transformed into less linearly separable representations. The position-wise analysis (Figure 6) also shows no substantial changes in either the number of high-accuracy positions or their spatial distribution as layers progressed.

Text conditioning constructs linearly decodable representations. Figure 7 shows $acc_{l,t}$ across layers and token positions in the text input part of the language model. Results for aspects other than Node Color, Edge Direction, Multi-hop Path, and Node Count are provided in appendix C.3. For almost all aspects, accuracy increased sharply at tokens that specify the target nodes or edges. This suggests that the language model selectively aggregates information from image-position hidden states into text-position hidden states, conditioned on the text input. In contrast, aspects in the Global category showed relatively high accuracy from the first text token. This suggests that global information is aggregated even without explicit conditioning. Exceptionally, for Multi-hop Path, the improvement in probing accuracy remained limited throughout.

6 Causal Intervention

In § 5, we analyzed where visual information about diagrams is encoded inside the model as a linearly decodable representation. However, although probing suggests that such representations exist, it remains unclear whether the model actually uses them for reasoning. To test this, we selectively corrupt hidden states in the vision encoder output whose probing accuracy exceeds a threshold for as-

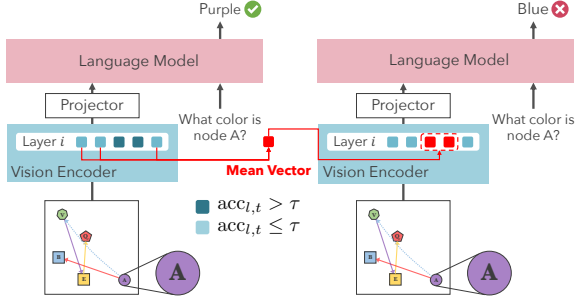


Figure 8: Overview of causal intervention. Hidden states of patches with probing accuracy exceeding the threshold are replaced with the mean of hidden states of other patches. If VQA accuracy decreases with this operation, it suggests that the replaced patch hidden states contributed to inference.

pect a before they are fed into the language model, and we measure the causal contribution as the resulting change in VQA performance.

6.1 Method

We conduct this experiment using the following procedure, as illustrated in Figure 8: (1) Identify target layers and positions for intervention. (2) Replace selected patch representations with the mean vector of other patches, corrupting hidden states with high probing accuracy. (3) Compare VQA accuracy before (clean run) and after (patched run) replacement (as described in § 4.1). As a control experiment to verify the validity of the intervention effect, we also compare performance when intervening at random positions.

Target layers. We apply intervention to the vision encoder layers that are input to the language model. Qwen3-VL 8B adopts the deepstack (Meng et al., 2024) architecture, where hidden states from intermediate layers (layers 8, 16, and 24) are input to the language model in addition to the output layer of the vision encoder. We perform intervention on all these input layers.

Target positions. Target positions for intervention are those where probing accuracy exceeds threshold τ . We replace all such target positions simultaneously in a single intervention.

For dataset $d_{\text{fix}} \in \mathcal{D}_{\text{test}}$ and layer l of the vision encoder, the set of target positions for intervention is defined as:

$$\mathcal{S}_{d_{\text{fix}}}^l = \{t \in \{1, \dots, T\} \mid \text{acc}_{l,t}(d_{\text{fix}}) > \tau\}, \quad (6)$$

where T is the total number of positions. The complement of $\mathcal{S}_{d_{\text{fix}}}^l$ is denoted as $\bar{\mathcal{S}}_{d_{\text{fix}}}^l$, represent-

ing the set of positions with accuracy at or below threshold τ .

Intervention operation. For each input x_i , we perform intervention with the following procedure. First, we compute the mean vector $\mu_{i,l}$ of hidden states at layer l with probing accuracy at or below threshold τ . Next, we replace the hidden states at intervention targets (positions $t \in \mathcal{S}_{d_{\text{fix}}}^l$) with this mean vector:

$$\mu_{i,l} = \text{mean}_{t \in \mathcal{S}_{d_{\text{fix}}}^l} \mathbf{h}_{i,l,t}, \quad (7)$$

$$\tilde{\mathbf{h}}_{i,l,t} = \begin{cases} \mu_{i,l} & (t \in \mathcal{S}_{d_{\text{fix}}}^l), \\ \mathbf{h}_{i,l,t} & (t \notin \mathcal{S}_{d_{\text{fix}}}^l). \end{cases} \quad (8)$$

We compare Acc_{VQA} when using $\mathbf{h}_{i,l,t}$ as input to the language model (clean run) with Acc_{VQA} when using $\tilde{\mathbf{h}}_{i,l,t}$ created by this operation (patched run).

Control experiment. To clarify whether the intervention effect truly results from intervening on hidden states with high probing accuracy, we evaluate accuracy changes when intervening at randomly selected positions as a control experiment. Specifically, we randomly sample the same number of positions as those where probing accuracy exceeds threshold τ ($= |\mathcal{S}_{d_{\text{fix}}}^l|$) and perform intervention on those positions. We select a set $\mathcal{R}_{d_{\text{fix}}}^l \subset \{1, \dots, T\}$ satisfying $|\mathcal{R}_{d_{\text{fix}}}^l| = |\mathcal{S}_{d_{\text{fix}}}^l|$ by sampling, and perform replacement as:

$$\tilde{\mathbf{h}}_{i,l,t} = \begin{cases} \mu_{i,l} & (t \in \mathcal{R}_{d_{\text{fix}}}^l), \\ \mathbf{h}_{i,l,t} & (t \notin \mathcal{R}_{d_{\text{fix}}}^l). \end{cases} \quad (9)$$

If accuracy when intervening on hidden states with high probing accuracy is lower compared to this control setting, we can judge that information encoded in hidden states with high probing accuracy causally contributes to model reasoning.

6.2 Results

Table 3 reports the results of causal interventions on Qwen3-VL 8B. For Node Color, Node Shape, Edge Color, Edge Style, Node Count, In-degree Count, and Out-degree Count, Acc_{VQA} decreased after the intervention. Furthermore, the reduction in Acc_{VQA} under the controlled setting was limited. These results indicate that, for these aspects, information from image-part hidden states whose probing accuracy exceeded the threshold τ causally contributed to inference. In contrast, for Edge Existence and Multi-hop Path, we did not observe a

	Node Color	Node Shape	In-degree Count	Out-degree Count	Edge Color	Edge Style	Edge Existence	Edge Direction	Multi-hop Path	Node Count
Clean run	91.4	76.6	40.3	34.7	57.3	73.5	69.6	49.3	58.3	40.3
Patched run	11.7	20.4	26.5	27.7	32.1	68.1	69.4	48.8	57.0	25.7
Controlled	83.4	73.6	36.8	34.3	53.8	72.3	68.6	50.3	57.1	31.8
Chance level	12.5	20.0	20.0	20.0	12.5	50.0	50.0	50.0	50.0	20.0
Δ (Clean run - Patched run)	79.7	56.2	13.8	7.0	25.2	5.4	0.2	0.5	1.3	14.6
Δ (Clean run - Controlled)	8.0	3.0	3.5	0.4	3.5	1.2	1.0	-1.0	1.2	8.5
Patched ratio	19.1	17.3	27.7	22.9	16.8	9.38	3.52	0.625	8.98	89.6

Table 3: Results of causal intervention on Qwen3-VL 8B. Clean run shows VQA accuracy without intervention. Patched run shows accuracy when all patches exceeding the threshold in probing accuracy are replaced. Controlled refers to the controlled experiment setting described in § 6.1.

decrease in Acc_{VQA} due to the intervention. This suggests that the model may rely on information that is encoded nonlinearly for inference. For Edge Direction, the model’s accuracy is already near chance level, indicating that it cannot answer these questions; thus, Acc_{VQA} is expected to remain unchanged regardless of the intervention. Moreover, for Edge Count, since $acc_{l,t} > \tau$ held for all probes subject to intervention, we could not construct the mean vector $\mu_{i,l}$ and therefore excluded this aspect.

7 Related Work

7.1 Diagram Understanding

Prior work has developed diagram understanding systems for tasks such as VQA (Lu et al., 2024; Wang et al., 2024) and image captioning (Hsu et al., 2021; Huang et al., 2023). While classical approaches relied on rule-based methods such as pattern matching and predefined schemas (Blostein, 1996; Song et al., 2017), methods using LVLMS are now mainstream.

Understanding diagrams requires recognizing visual elements such as symbols and shapes, and capturing their relationships. Studies (Pan et al., 2024; Zhu et al., 2025; Hou et al., 2025) demonstrate that LVLMS recognize these elements adequately, while they struggle to capture relationships. The underlying cause of this limitation is unclear.

Our work clarifies a contributing factor to this problem by analyzing how LVLMS internally represent diagram elements and their relationships.

7.2 Internal Analysis of LVLMS

To understand how LVLMS process visual information, Gandelsman et al. (2024) and Tao et al. (2024) analyze internal representations. For example, Gandelsman et al. (2024) analyzed how natural images are represented within CLIP (Radford et al.,

2021), a widely used vision encoder for LVLMS. They revealed that multiple attention heads capture specific properties such as color, shape, and number. They also found that visual information localizes in patches corresponding to specific image regions. Additionally, Tao et al. (2024) analyzed global and local semantic information within the language model of LVLMS for natural images. They revealed that middle layers encode global information, while later layers encode local information.

In contrast, our work analyzes the internal representations of LVLMS for diagrams, which, unlike natural images, represent information symbolically through text and shapes and structurally through relationships such as edge connectivity.

8 Conclusion

We construct a synthetic diagram dataset and conduct probing and causal intervention analyses to clarify how visual information in diagrams is processed and differentiated within LVLMS. Our probing results reveal that the processing stage at which representations become linearly separable depends on the type of visual information. Specifically, node information and global information are linearly encoded within single image patches in the vision encoder, whereas edge relationship is not linearly separable in the vision encoder and becomes linearly encoded only in text tokens in the language model. Causal intervention experiments further confirm that visual information linearly encoded in the vision encoder has a causal effect during inference. These findings demonstrate that LVLMS process different types of visual information in distinct ways, and suggest that such representational differences may contribute to challenges in recognizing relational structure between diagram elements.

Limitations

Coverage of real-world diagrams. We use synthetic diagrams to minimize the influence of dataset biases and shortcut learning that can arise from natural-language and natural-image data. Although using a synthetic dataset enables well-controlled and fine-grained analysis, our setup does not necessarily capture all complex situations found in real-world diagrams.

In addition, we focus on basic visual information, such as node color and shape, and edge direction. Although complex information may be represented by combining these cues, how the model represents composite visual patterns and higher-order structures remains unexamined.

Probing methods. Probing-based approaches for interpreting the internal mechanisms of language models have been widely studied in our field (Conneau et al., 2018; Tenney et al., 2019; Campbell et al., 2023; Li et al., 2023). However, there are some criticisms regarding the validity of probing approaches (Liu et al., 2023; Burns et al., 2023). We also consider it a viable option to adopt a broader range of probing methods (Gurnee et al., 2023; Bricken et al., 2023).

Ethics statement

We do not anticipate any significant ethical concerns because (i) we conducted no human-subject experiments, and (ii) our tasks involve only simple, synthetically generated diagrams and do not address ethically sensitive topics.

Acknowledgments

This work was supported by JST CREST Grant Number JPMJCR20D2, JST PREST Grant Number JPMJFR242S, JST SPRING Grant Number JPMJSP2114, and JSPS KAKENHI Grant Numbers JP24K20829, JP25K03175, JP25KJ0615. We would also like to express our sincere gratitude to the members of the Tohoku NLP Group for their invaluable advice and support throughout this research.

References

Takuya Akiba, Shotaro Sano, Toshihiko Yanase, Takeru Ohta, and Masanori Koyama. 2019. Optuna: A next-generation hyperparameter optimization framework. In *Proceedings of the 25th ACM SIGKDD International Conference on Knowledge Discovery & Data*

Mining, KDD '19, page 2623–2631, New York, NY, USA. Association for Computing Machinery.

Guillaume Alain and Yoshua Bengio. 2017. Understanding intermediate layers using linear classifier probes.

Shuai Bai, Yuxuan Cai, Ruizhe Chen, Keqin Chen, Xionghui Chen, Zesen Cheng, Lianghao Deng, Wei Ding, Chang Gao, Chunjiang Ge, Wenbin Ge, Zhifang Guo, Qidong Huang, Jie Huang, Fei Huang, Binyuan Hui, Shutong Jiang, Zhaohai Li, Mingsheng Li, and 45 others. 2025a. Qwen3-VL technical report.

Shuai Bai, Keqin Chen, Xuejing Liu, Jialin Wang, Wenbin Ge, Sibao Song, Kai Dang, Peng Wang, Shijie Wang, Jun Tang, Humen Zhong, Yuanzhi Zhu, Mingkun Yang, Zhaohai Li, Jianqiang Wan, Pengfei Wang, Wei Ding, Zheren Fu, Yiheng Xu, and 8 others. 2025b. Qwen2.5-VL technical report.

B Berlin and P Kay. 1999. *Basic Color Terms: Their Universality and Evolution*. The David Hume Series. Cambridge University Press, Cambridge, England.

Dorothea Blostein. 1996. General diagram-recognition methodologies. In *Graphics Recognition Methods and Applications*, pages 106–122, Berlin, Heidelberg. Springer Berlin Heidelberg.

Trenton Bricken, Adly Templeton, Joshua Batson, Brian Chen, Adam Jermy, Tom Conerly, Nick Turner, Cem Anil, Carson Denison, Amanda Askell, Robert Lasenby, Yifan Wu, Shauna Kravec, Nicholas Schiefer, Tim Maxwell, Nicholas Joseph, Zac Hatfield-Dodds, Alex Tamkin, Karina Nguyen, and 6 others. 2023. Towards monosemanticity: Decomposing language models with dictionary learning. *Transformer Circuits Thread*.

Collin Burns, Haotian Ye, Dan Klein, and Jacob Steinhardt. 2023. Discovering latent knowledge in language models without supervision. In *The Eleventh International Conference on Learning Representations*.

James Campbell, Phillip Guo, and Richard Ren. 2023. Localizing lying in llama: Understanding instructed dishonesty on true-false questions through prompting, probing, and patching. In *Socially Responsible Language Modelling Research*.

Alexis Conneau, German Kruszewski, Guillaume Lample, Loïc Barrault, and Marco Baroni. 2018. What you can cram into a single $\&\!#*$ vector: Probing sentence embeddings for linguistic properties. In *Proceedings of the 56th Annual Meeting of the Association for Computational Linguistics (Volume 1: Long Papers)*, pages 2126–2136, Melbourne, Australia. Association for Computational Linguistics.

Corentin Dancette, Rémi Cadène, Damien Teney, and Matthieu Cord. 2021. Beyond question-based biases: Assessing multimodal shortcut learning in visual question answering. In *2021 IEEE/CVF Interna-*

- tional Conference on Computer Vision (ICCV)*, pages 1554–1563.
- Timothée Darcet, Maxime Oquab, Julien Mairal, and Piotr Bojanowski. 2024. Vision transformers need registers. In *The Twelfth International Conference on Learning Representations*.
- Alexey Dosovitskiy, Lucas Beyer, Alexander Kolesnikov, Dirk Weissenborn, Xiaohua Zhai, Thomas Unterthiner, Mostafa Dehghani, Matthias Minderer, Georg Heigold, Sylvain Gelly, Jakob Uszkoreit, and Neil Houlsby. 2021. An image is worth 16x16 words: Transformers for image recognition at scale. In *International Conference on Learning Representations*.
- Yossi Gandelsman, Alexei A Efros, and Jacob Steinhardt. 2024. Interpreting CLIP’s image representation via text-based decomposition. In *The Twelfth International Conference on Learning Representations*.
- Wes Gurnee, Neel Nanda, Matthew Pauly, Katherine Harvey, Dmitrii Troitskii, and Dimitris Bertsimas. 2023. Finding neurons in a haystack: Case studies with sparse probing. *Transactions on Machine Learning Research*.
- Suchin Gururangan, Swabha Swayamdipta, Omer Levy, Roy Schwartz, Samuel Bowman, and Noah A Smith. 2018. Annotation artifacts in natural language inference data. In *Proceedings of the 2018 Conference of the North American Chapter of the Association for Computational Linguistics: Human Language Technologies, Volume 2 (Short Papers)*, pages 107–112, New Orleans, Louisiana. Association for Computational Linguistics.
- Jennifer Healey, Laurie Byrum, Md Nadeem Akhtar, and Moumita Sinha. 2024. Evaluating nuanced bias in large language model free response answers. In *Natural Language Processing and Information Systems*, pages 378–391, Cham. Springer Nature Switzerland.
- John Hewitt and Percy Liang. 2019. Designing and interpreting probes with control tasks. In *Proceedings of the 2019 Conference on Empirical Methods in Natural Language Processing and the 9th International Joint Conference on Natural Language Processing (EMNLP-IJCNLP)*, pages 2733–2743, Hong Kong, China. Association for Computational Linguistics.
- Yifan Hou, Buse Giledereli, Yilei Tu, and Mrinmaya Sachan. 2025. Do vision-language models really understand visual language? In *Forty-second International Conference on Machine Learning*.
- Ting-Yao Hsu, C Lee Giles, and Ting-Hao Huang. 2021. SciCap: Generating captions for scientific figures. In *Findings of the Association for Computational Linguistics: EMNLP 2021*, pages 3258–3264, Punta Cana, Dominican Republic. Association for Computational Linguistics.
- Chieh-Yang Huang, Ting-Yao Hsu, Ryan Rossi, Ani Nenkova, Sungchul Kim, Gromit Yeuk-Yin Chan, Eunyee Koh, Clyde Lee Giles, and Ting-Hao ‘Kenneth’ Huang. 2023. Summaries as captions: Generating figure captions for scientific documents with automated text summarization. In *Proceedings of the 16th International Natural Language Generation Conference*, pages 80–92, Prague, Czechia. Association for Computational Linguistics.
- Gregor Jošt, Jernej Huber, Marjan Heričko, and Gregor Polančič. 2017. Improving cognitive effectiveness of business process diagrams with opacity-driven graphical highlights. *Decision Support Systems*, 103:58–69.
- Kushal Kafle and Christopher Kanan. 2017. An analysis of visual question answering algorithms. In *2017 IEEE International Conference on Computer Vision (ICCV)*, pages 1983–1991.
- Aniruddha Kembhavi, Mike Salvato, Eric Kolve, Minjoon Seo, Hannaneh Hajishirzi, and Ali Farhadi. 2016. A diagram is worth a dozen images. In *Computer Vision – ECCV 2016*, pages 235–251, Cham. Springer International Publishing.
- Sebastian Kernbach and Martin J Eppler. 2010. The use of visualization in the context of business strategies: An experimental evaluation. In *2010 14th International Conference Information Visualisation*, pages 349–354.
- Kurt W Kohn and Mirit I Aladjem. 2006. Circuit diagrams for biological networks. *Molecular Systems Biology*, 2(1):MSB4100044.
- Kenneth Li, Aspen K Hopkins, David Bau, Fernanda Viégas, Hanspeter Pfister, and Martin Wattenberg. 2023. Emergent world representations: Exploring a sequence model trained on a synthetic task. In *The Eleventh International Conference on Learning Representations*.
- Xue Li, Yiyu Sun, Wei Cheng, Yinglun Zhu, and Haifeng Chen. 2025. Chain-of-region: Visual language models need details for diagram analysis. In *The Thirteenth International Conference on Learning Representations*.
- Haotian Liu, Chunyuan Li, Yuheng Li, and Yong Jae Lee. 2024. Improved baselines with visual instruction tuning. In *2024 IEEE/CVF Conference on Computer Vision and Pattern Recognition (CVPR)*, pages 26286–26296.
- Kevin Liu, Stephen Casper, Dylan Hadfield-Menell, and Jacob Andreas. 2023. Cognitive dissonance: Why do language model outputs disagree with internal representations of truthfulness? In *Proceedings of the 2023 Conference on Empirical Methods in Natural Language Processing*, pages 4791–4797, Singapore. Association for Computational Linguistics.

- Pan Lu, Hritik Bansal, Tony Xia, Jiacheng Liu, Chunyuan Li, Hannaneh Hajishirzi, Hao Cheng, Kai-Wei Chang, Michel Galley, and Jianfeng Gao. 2024. MathVista: Evaluating mathematical reasoning of foundation models in visual contexts. In *The Twelfth International Conference on Learning Representations*.
- Lingchen Meng, Jianwei Yang, Rui Tian, Xiyang Dai, Zuxuan Wu, Jianfeng Gao, and Yu-Gang Jiang. 2024. DeepStack: Deeply stacking visual tokens is surprisingly simple and effective for LMMs. In *The Thirty-eighth Annual Conference on Neural Information Processing Systems*.
- Huitong Pan, Qi Zhang, Cornelia Caragea, Eduard C Dragut, and Longin Jan Latecki. 2024. FlowLearn: Evaluating large vision-language models on flowchart understanding. In *ECAI 2024 - 27th European Conference on Artificial Intelligence, 19-24 October 2024, Santiago de Compostela, Spain - Including 13th Conference on Prestigious Applications of Intelligent Systems (PAIS 2024)*, volume 392 of *Frontiers in Artificial Intelligence and Applications*, pages 73–80. IOS Press.
- Alec Radford, Jong Wook Kim, Chris Hallacy, Aditya Ramesh, Gabriel Goh, Sandhini Agarwal, Girish Sastry, Amanda Askell, Pamela Mishkin, Jack Clark, Gretchen Krueger, and Ilya Sutskever. 2021. Learning transferable visual models from natural language supervision. In *Proceedings of the 38th International Conference on Machine Learning*, volume 139 of *Proceedings of Machine Learning Research*, pages 8748–8763. PMLR.
- Samuel Silva, Beatriz Sousa Santos, and Joaquim Madeira. 2011. Using color in visualization: A survey. *Computers & Graphics*, 35(2):320–333.
- Dan Song, Dongming Wang, and Xiaoyu Chen. 2017. Retrieving geometric information from images: the case of hand-drawn diagrams. *Data Mining and Knowledge Discovery*, 31(4):934–971.
- Anna Sterzik, Nils Lichtenberg, Jana Wilms, Michael Krone, Douglas W Cunningham, and Kai Lawonn. 2024. Perception of line attributes for visualization. *IEEE Transactions on Visualization and Computer Graphics*, 30(1):1041–1051.
- Mingxu Tao, Quzhe Huang, Kun Xu, Liwei Chen, Yansong Feng, and Dongyan Zhao. 2024. Probing multimodal large language models for global and local semantic representations. In *Proceedings of the 2024 Joint International Conference on Computational Linguistics, Language Resources and Evaluation (LREC-COLING 2024)*, pages 13050–13056, Torino, Italia. ELRA and ICCL.
- Gemma Team, Aishwarya Kamath, Johan Ferret, Shreya Pathak, Nino Vieillard, Ramona Merhej, Sarah Perrin, Tatiana Matejovicova, Alexandre Ramé, Morgane Rivière, Louis Rouillard, Thomas Mesnard, Geoffrey Cideron, Jean-Bastien Grill, Sabela Ramos, Edouard Yvinec, Michelle Casbon, Etienne Pot, Ivo Penchev, and 197 others. 2025. Gemma 3 technical report.
- Ian Tenney, Patrick Xia, Berlin Chen, Alex Wang, Adam Poliak, R Thomas McCoy, Najoung Kim, Benjamin Van Durme, Sam Bowman, Dipanjan Das, and Ellie Pavlick. 2019. What do you learn from context? probing for sentence structure in contextualized word representations. In *International Conference on Learning Representations*.
- Chin Tseng, Arran Zeyu Wang, Ghulam Jilani Quadri, and Danielle Albers Szafrir. 2025. Shape it up: An empirically grounded approach for designing shape palettes. *IEEE Transactions on Visualization and Computer Graphics*, 31(1):349–359.
- Shaowei Wang, Lingling Zhang, Longji Zhu, Tao Qin, Kim-Hui Yap, Xinyu Zhang, and Jun Liu. 2024. CoG-DQA: Chain-of-guiding learning with large language models for diagram question answering. In *2024 IEEE/CVF Conference on Computer Vision and Pattern Recognition (CVPR)*, pages 13969–13979.
- Fred Zhang and Neel Nanda. 2024. Towards best practices of activation patching in language models: Metrics and methods. In *The Twelfth International Conference on Learning Representations*.
- Renrui Zhang, Dongzhi Jiang, Yichi Zhang, Haokun Lin, Ziyu Guo, Pengshuo Qiu, Aojun Zhou, Pan Lu, Kai-Wei Chang, Yu Qiao, Peng Gao, and Hongsheng Li. 2025. MATHVERSE: Does your multi-modal LLM truly see the diagrams in visual math problems? In *Computer Vision – ECCV 2024*, pages 169–186, Cham. Springer Nature Switzerland.
- Yingjie Zhu, Xuefeng Bai, Kehai Chen, Yang Xiang, Jun Yu, and Min Zhang. 2025. Benchmarking and improving large vision-language models for fundamental visual graph understanding and reasoning. In *Proceedings of the 63rd Annual Meeting of the Association for Computational Linguistics (Volume 1: Long Papers)*, pages 30678–30701, Vienna, Austria. Association for Computational Linguistics.

A Details of VQA Evaluation Setup

Table 4 shows the questions used to evaluate each aspect in our experiments.

B Dataset

B.1 Detailed Dataset Specification

The color candidates for nodes and edges were selected from the Basic Color Terms (11 colors) defined by Berlin and Kay (1999), excluding white, black, and gray, resulting in eight colors. The shape candidates for nodes were chosen as basic geometric figures that do not strongly evoke specific meanings, including circles and regular polygons. We excluded equilateral triangles because their shape resembles edge arrowheads, which could cause confusion between nodes and edges.

C Probing

C.1 Shortcut learning of probe

In the probing experiments, we observed shortcuts across all aspects where the probe predicted answers based solely on superficial features of the input patches. These shortcuts resulted in 100% accuracy on patches in certain regions. For example, for the node color aspect, the probe achieved 100% accuracy on patches containing the target node by simply predicting the color of the input patch. Beyond node color, we also confirmed shortcuts that exploited information such as patch shape and position.

These shortcuts do not reflect correct understanding of the diagram’s visual information. To correctly classify the node color aspect, the probe must first identify node A and then predict its color. However, shortcut-based predictions skip the identification of node A. This phenomenon occurs because the probe determines that predicting superficial features of input patches maximizes overall accuracy based on the dataset distribution.

To address this problem, as described in § 3.3, we add diagrams without node A as dummy data to the training dataset. This approach ensures that when the input does not contain the information necessary for prediction, the probe outputs the dummy class (N/A), thereby avoiding falsely high accuracy through shortcuts.

C.2 Probe Training Hyperparameters

We used linear classifiers for probe training, training separately for each aspect. The hyperparam-

eters differed only in batch size between image-part probing and text-part probing. Table 5 shows the hyperparameters used for each type of probing.

For hyperparameter search, we used Optuna (Akiba et al., 2019) with TPESampler to perform three hyperparameter search trials. The search targets were batch size and learning rate, where batch size was selected categorically from the candidates shown in Table 5, and learning rate was searched on a log scale ranging from 0.0001 to 0.01. For the evaluation metric, we split 10% of the training data as validation data and used accuracy on the validation data. We did not use early stopping during training; instead, we evaluated performance on the validation data at each epoch and saved the model that achieved the highest accuracy.

C.3 Additional results

In this section, we present additional analysis results beyond the Qwen3-VL 8B results reported in the main text. Specifically, we report detailed probing results for Qwen3-VL 8B and results with different node layouts, as well as probing results for additional models (Qwen2.5-VL 7B, LLaVA1.5 7B, Gemma3-4B-IT).

Qwen3-VL 8B (detailed probing results). Figure 9 and Figure 10 present image probing results with two additional intermediate layers that were omitted in Figure 4 and Figure 6. As described in § 5.3, Single category information is encoded near node positions, while Global category information is distributed across background regions. Figure 11 presents text probing results for aspects omitted from Figure 7. As described in § 5.3, accuracy sharply increased at token positions that specify the target nodes or edges.

Qwen3-VL 8B (different node layouts). Figure 13 and Figure 14 show results with different node layouts (see Figure 12). In the main text, we placed the target node (node A) at the bottom-right, but here we show results with node A placed on the left side. The distribution of patches with high accuracy for node information changed according to the position of node A. This result demonstrates that the probe appropriately captures positional information of the target node.

Qwen2.5-VL 7B. Figure 15 through Figure 18 show the probing results for Qwen2.5-VL 7B. The overall trends are similar to Qwen3-VL, with node information showing high accuracy while edge rela-

Aspect	Question
Node Color	What color is node A?
Node Shape	What shape is node A?
In-degree	What is the in-degree of node A?
Out-degree	What is the out-degree of node A?
Edge Color	What color is the edge between node A and node B?
Edge Style	What style is the edge between node A and node B?
Edge Existence	Does an edge exist between node A and node B?
Edge Direction	What is the direction of the edge between node A and node B?
Multi-hop Path	Is there a path from node A to node B?
Node Count	How many nodes labeled A are in the graph?
Edge Count	How many edges are in the graph?

Table 4: Questions used to evaluate each aspect.

Parameter	Image Part	Text Part
Epochs	1000	1000
Batch size*	{1000, 2000, 4000, 8000, 16000}	{10, 20, 40, 80, 160}
Learning rate*	[0.0001, 0.01] (log scale)	[0.0001, 0.01] (log scale)
Optimizer	AdamW	AdamW
betas	[0.9, 0.999]	[0.9, 0.999]
eps	1e-08	1e-08
weight decay	0.01	0.01

Table 5: Hyperparameters used for probe training. Batch size and learning rate were subject to hyperparameter search using Optuna. Optimizer parameters use PyTorch’s AdamW default values. *Subject to hyperparameter search

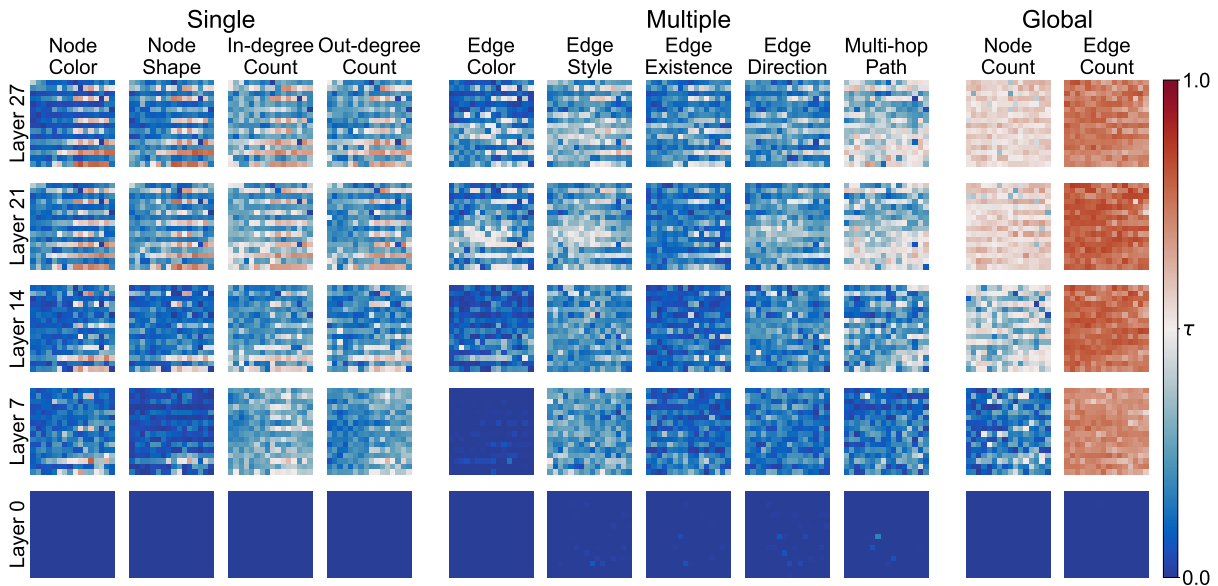


Figure 9: Accuracy for each hidden state in the image input part of the Qwen3-VL 8B vision encoder. Each heatmap shows the accuracy of individual hidden states for a specific layer and aspect.

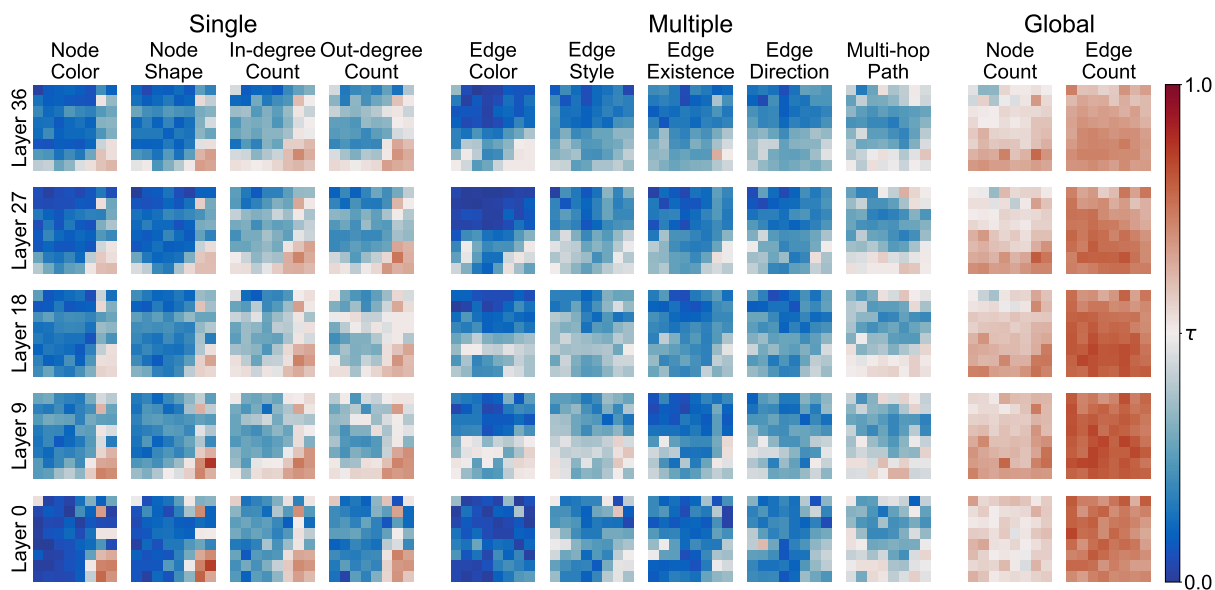


Figure 10: Accuracy for each hidden state in the image input part of the Qwen3-VL 8B language model. Each heatmap shows the accuracy of individual hidden states for a specific layer and aspect.

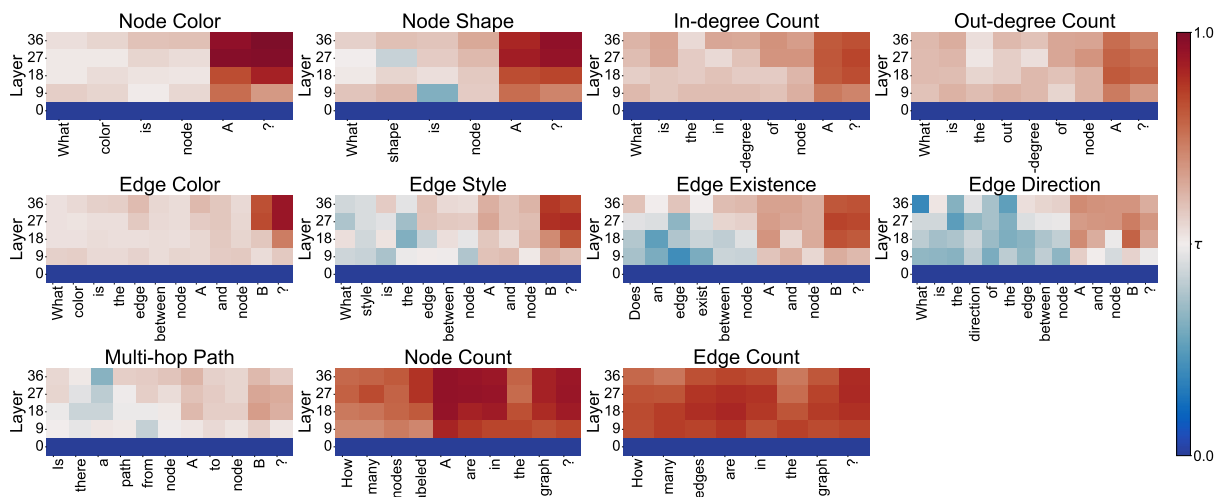


Figure 11: Probing results for text tokens in Qwen3-VL 8B. The x-axis shows token position in the question, and the y-axis shows layer position.

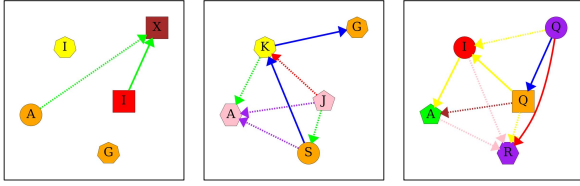


Figure 12: Example diagrams with layouts distinct from those in Figure 2.

tionships remained near chance level. In the patch-wise analysis, patches corresponding to node positions showed higher accuracy compared to background patches.

Figure 19 shows the probing results for text tokens. Similar to Qwen3-VL, we observed a trend where accuracy sharply increased at token positions that specify nodes or edges.

LLaVA1.5 7B. Figure 20 through Figure 24 show the results for LLaVA1.5 7B. The overall trends are similar to Qwen3-VL and Qwen2.5-VL, but a distinctive difference was observed in the patch-wise analysis. In LLaVA1.5, background patches showed higher accuracy than patches corresponding to node positions. This result indicates that LLaVA1.5 aggregates visual information into background patches.

Figure 24 shows the probing results for text tokens. Similar to other models, we observed information aggregation at token positions that specify target nodes or edges.

Gemma3-4B-IT. Figure 25 through Figure 29 show the probing results for Gemma3-4B-IT. The overall trends are similar to Qwen3-VL and Qwen2.5-VL, but accuracy was lower for some node information and edge relationships compared to other models.

Figure 29 shows the probing results for text tokens. As with the other models, we observe an aggregation of information at the token positions that specify the target nodes or edges; however, the effect is weaker than in the other models.

D Additional results for Causal intervention

In the main text, we reported the causal intervention results for our primary model, Qwen3-VL 8B (§ 6). In this section, we present results for additional models (Qwen2.5-VL 7B, LLaVA1.5 7B, and Gemma3-4B-IT).

Table 6 shows the results for Qwen2.5-VL 7B.

Similar to Qwen3-VL, the intervention caused a large drop in accuracy for node information such as node color and node shape. In addition, the intervention also degraded performance on node count, suggesting that globally encoded information that is linearly represented in the vision encoder contributes to reasoning.

Table 7 reports the results for LLaVA1.5 7B. Although LLaVA1.5 has lower baseline VQA performance than the other models, we still observe a performance drop after the intervention for aspects such as node color and edge color. However, for some aspects, the fraction of patched positions is extremely high (e.g., 89.8% for node color), suggesting that information about these aspects is broadly distributed across patches, including background regions.

Table 8 reports the results for Gemma3-4B-IT. We observe a drop in performance after intervening on Node Color and Node Shape, indicating that linearly decodable information in the vision encoder contributes to VQA reasoning. For Gemma3, the fraction of replaced hidden states is relatively small (e.g., 7.55% for Node Color), suggesting that node-attribute information is encoded more locally.

Across all models, applying causal interventions to features that are linearly represented in the vision encoder (e.g., node information and global information) consistently reduced performance. This suggests that the linear representations identified by probing are not only present, but also causally used for inference. In contrast, for aspects that are not well captured by linear decoding in the vision encoder, such as edge direction, the intervention caused little to no change in performance. This pattern suggests that the model may rely on nonlinearly encoded information or on other mechanisms beyond the probed linear features.

E Computational resources

We used NVIDIA RTX 6000 Ada, RTX PRO 6000 Blackwell Max-Q, and H100 GPUs in this study.

F Usage of AI assistants

For writing this paper and developing the experimental code, we used AI assistants (e.g., ChatGPT and GitHub Copilot). Their use was limited to tasks such as code completion, translation, text editing, and table formatting, and all technical content is based solely on the authors’ ideas.

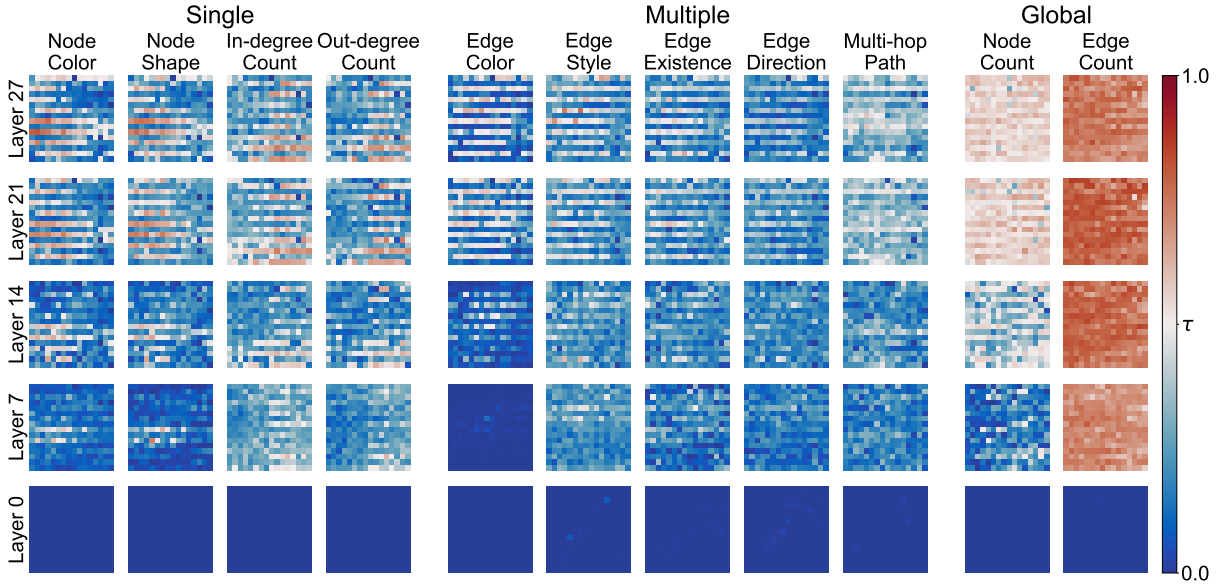


Figure 13: Accuracy for each hidden state in the image input part of the Qwen3-VL 8B vision encoder (node A placed on the left side). Each heatmap shows the accuracy of individual hidden states for a specific layer and aspect.

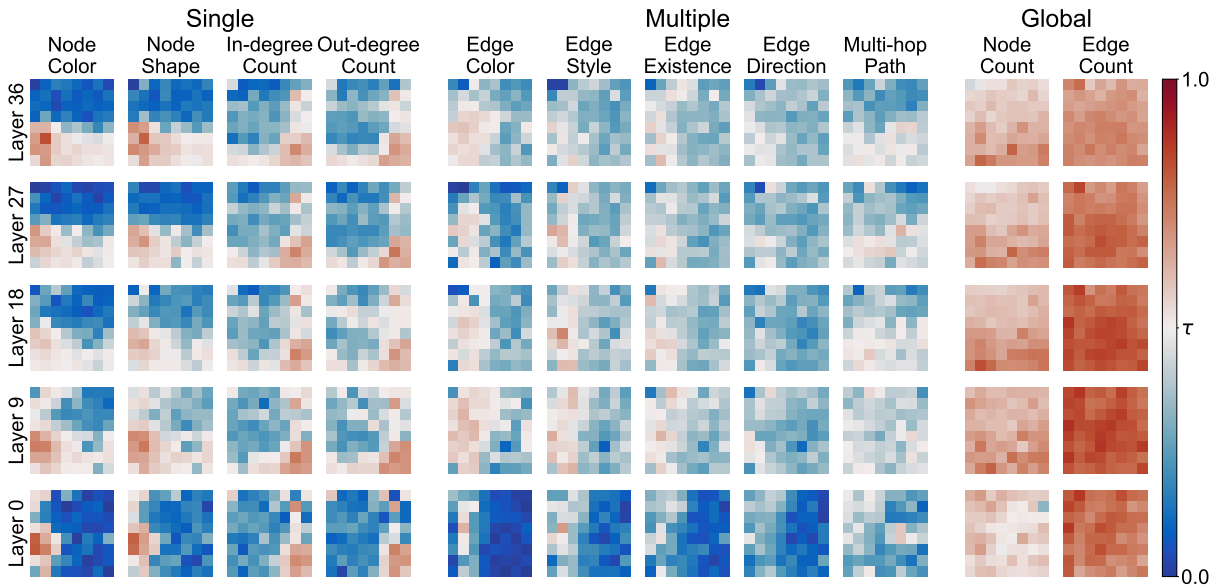


Figure 14: Accuracy for each hidden state in the image input part of the Qwen3-VL 8B language model (node A placed on the left side). Each heatmap shows the accuracy of individual hidden states for a specific layer and aspect.

	Node Color	Node Shape	In-degree Count	Out-degree Count	Edge Color	Edge Style	Edge Existence	Edge Direction	Multi-hop Path	Node Count	Edge Count
Clean run	91.9	78.0	37.0	28.8	54.9	71.0	50.0	46.0	65.0	83.6	22.2
Patched run	11.9	20.4	25.0	21.8	40.9	73.0	50.5	47.0	51.0	17.2	N/A
Controlled	93.4	78.0	37.4	26.8	56.6	69.0	50.0	45.0	69.5	21.0	N/A
Chance level	12.5	20.0	20.0	20.0	12.5	50.0	50.0	50.0	50.0	20.0	20.0
Patched ratio	28.5	22.3	37.9	31.6	16.0	8.20	3.50	1.56	28.1	93.0	100

Table 6: Results of the causal intervention for Qwen2.5-VL 7B. “Patched” reports the results when all hidden states whose probing accuracy exceeded the threshold were replaced. “Controlled” reports the results when the same number of patches as those whose probing accuracy exceeded the threshold were randomly selected and replaced.

	Node Color	Node Shape	In-degree Count	Out-degree Count	Edge Color	Edge Style	Edge Existence	Edge Direction	Multi-hop Path	Node Count	Edge Count
Clean run	40.5	39.6	34.0	30.8	38.1	49.5	60.5	50.0	50.0	20.0	27.2
Patched run	49.6	28.8	71.2	52.8	16.0	50.5	59.5	50.0	50.0	21.8	N/A
Controlled	9.20	19.6	20.0	22.4	13.0	50.0	59.0	50.0	50.0	21.2	N/A
Chance level	12.5	20.0	20.0	20.0	12.5	50.0	50.0	50.0	50.0	20.0	20.0
Patched ratio	89.8	83.5	94.4	93.9	75.3	11.1	0.174	0	65.3	99.8	100

Table 7: Causal intervention results for LLaVA1.5 7B. “Patched run” denotes the results when all patches whose probing accuracy exceeds the threshold are replaced. “Controlled” denotes the results when the same number of patches as those exceeding the threshold are randomly selected and replaced.

	Node Color	Node Shape	In-degree Count	Out-degree Count	Edge Color	Edge Style	Edge Existence	Edge Direction	Multi-hop Path	Node Count	Edge Count
Clean run	69.2	50.0	26.4	30.0	41.2	57.2	56.6	50.3	50.0	33.9	20.1
Patched run	35.8	33.6	25.1	27.0	41.0	56.9	57.0	50.1	50.0	9.40	20.5
Controlled	68.2	48.3	25.7	29.8	40.8	57.2	56.9	49.9	50.0	23.9	20.6
Chance level	12.5	20.0	20.0	20.0	12.5	50.0	50.0	50.0	50.0	20.0	20.0
Patched ratio	7.55	5.44	7.06	6.28	0.708	1.34	0.457	0.425	11.0	72.3	82.4

Table 8: Causal intervention results for Gemma3-4B-IT. “Patched run” reports the results when all hidden states whose probing accuracy exceeded the threshold are replaced. “Controlled” reports the results when the same number of hidden states as those exceeding the probing-accuracy threshold is randomly selected and replaced.

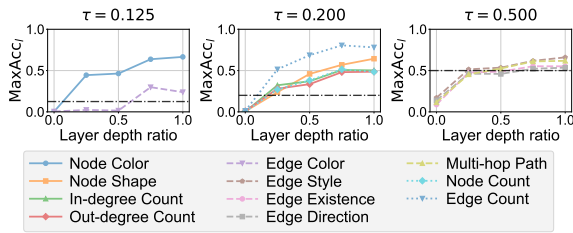


Figure 15: Layer-wise maximum accuracy in the vision encoder of Qwen2.5-VL 7B. The x-axis shows relative layer position (0 is the input layer, 1 is the final layer), and the y-axis shows accuracy. The black dotted line indicates the threshold.

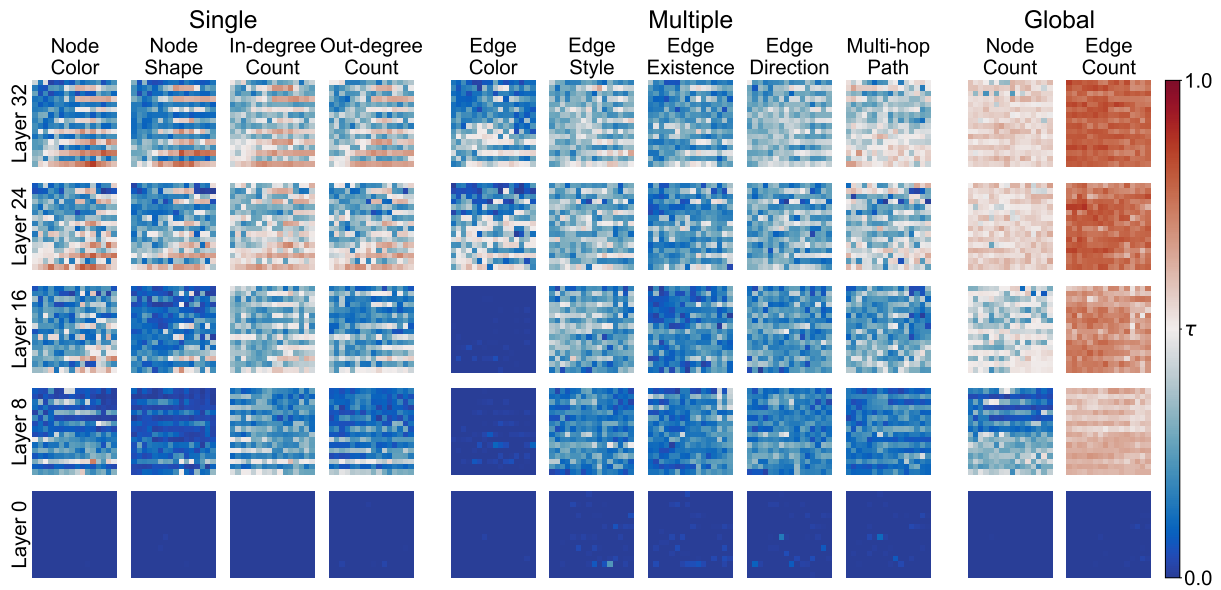


Figure 16: Accuracy for each hidden state in the image input part of the Qwen2.5-VL 7B vision encoder. Each heatmap shows the accuracy of individual hidden states for a specific layer and aspect.

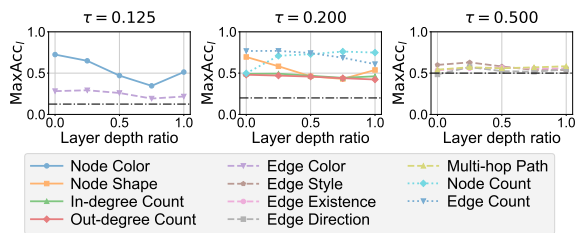


Figure 17: Layer-wise maximum accuracy in the language model of Qwen2.5-VL 7B. The x-axis shows relative layer position (0 is the input layer, 1 is the final layer), and the y-axis shows accuracy. The black dotted line indicates the threshold.

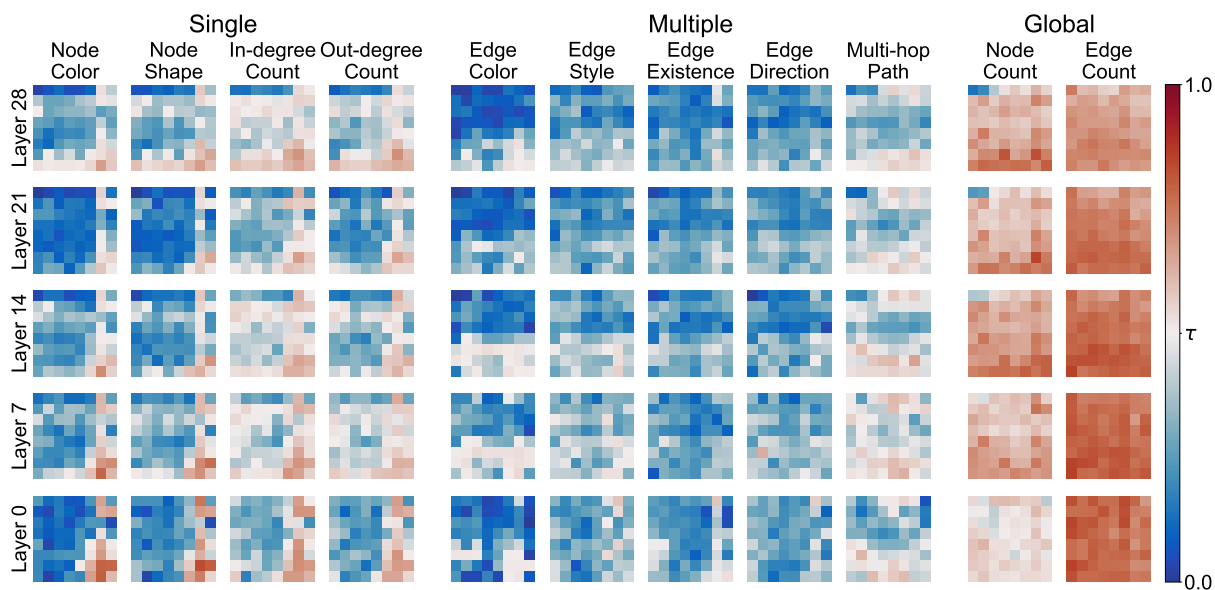


Figure 18: Accuracy for each hidden state in the image input part of the Qwen2.5-VL 7B language model. Each heatmap shows the accuracy of individual hidden states for a specific layer and aspect.

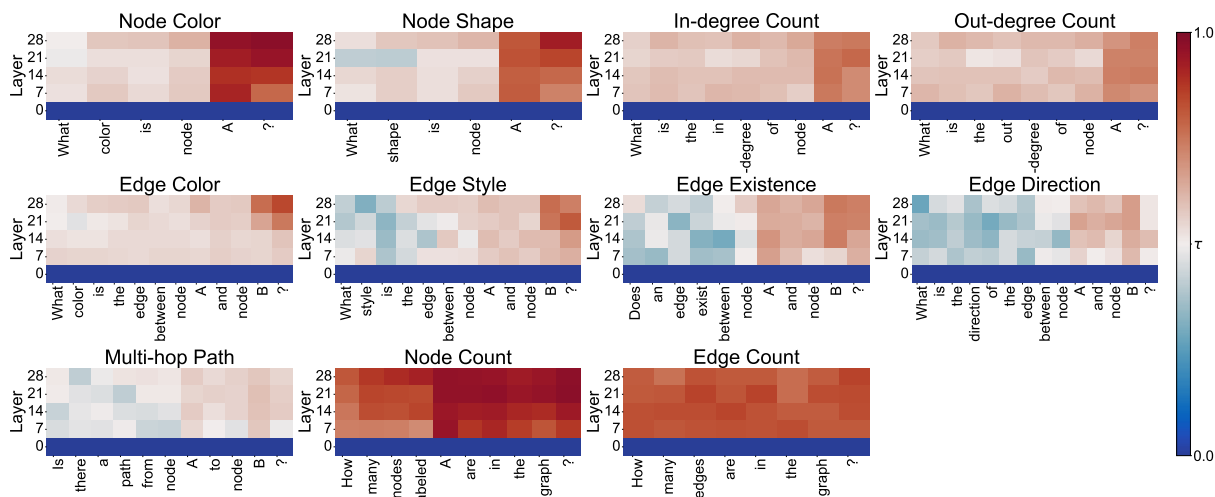


Figure 19: Probing results for text tokens in Qwen2.5-VL 7B. The x-axis shows token position in the question, and the y-axis shows layer position.

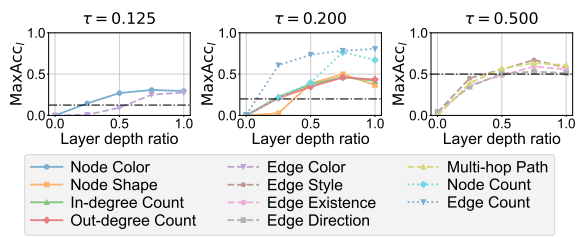


Figure 20: Layer-wise maximum accuracy in the vision encoder of LLaVA1.5 7B. The x-axis shows relative layer position (0 is the input layer, 1 is the final layer), and the y-axis shows accuracy. The black dotted line indicates the threshold.

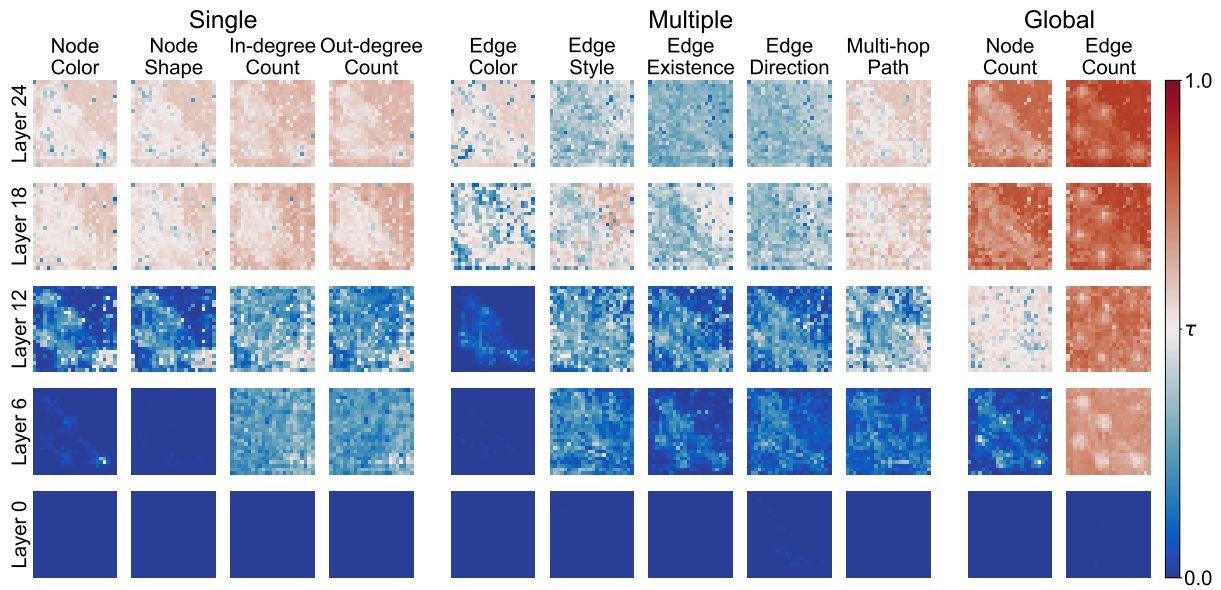


Figure 21: Accuracy for each hidden state in the image input part of the LLaVA1.5 7B vision encoder. Each heatmap shows the accuracy of individual hidden states for a specific layer and aspect.

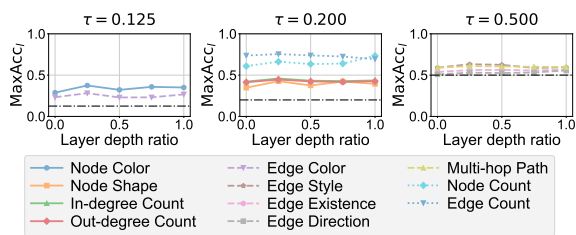


Figure 22: Layer-wise maximum accuracy in the language model of LLaVA1.5 7B. The x-axis shows relative layer position (0 is the input layer, 1 is the final layer), and the y-axis shows accuracy. The black dotted line indicates the threshold.

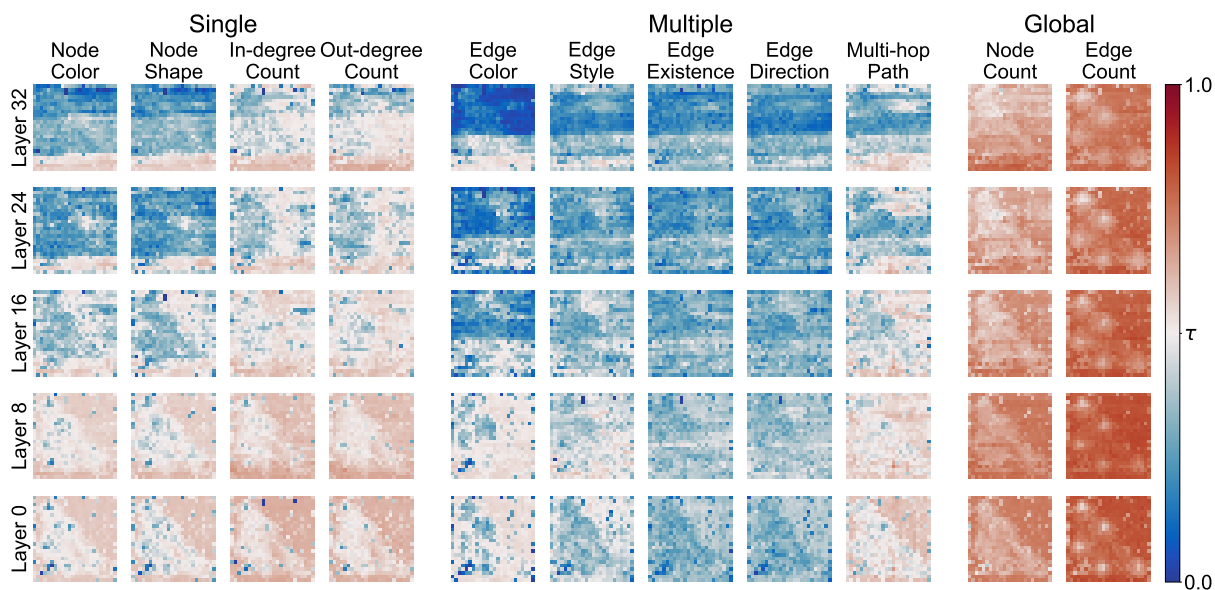


Figure 23: Accuracy for each hidden state in the image input part of the LLaVA1.5 7B language model. Each heatmap shows the accuracy of individual hidden states for a specific layer and aspect.

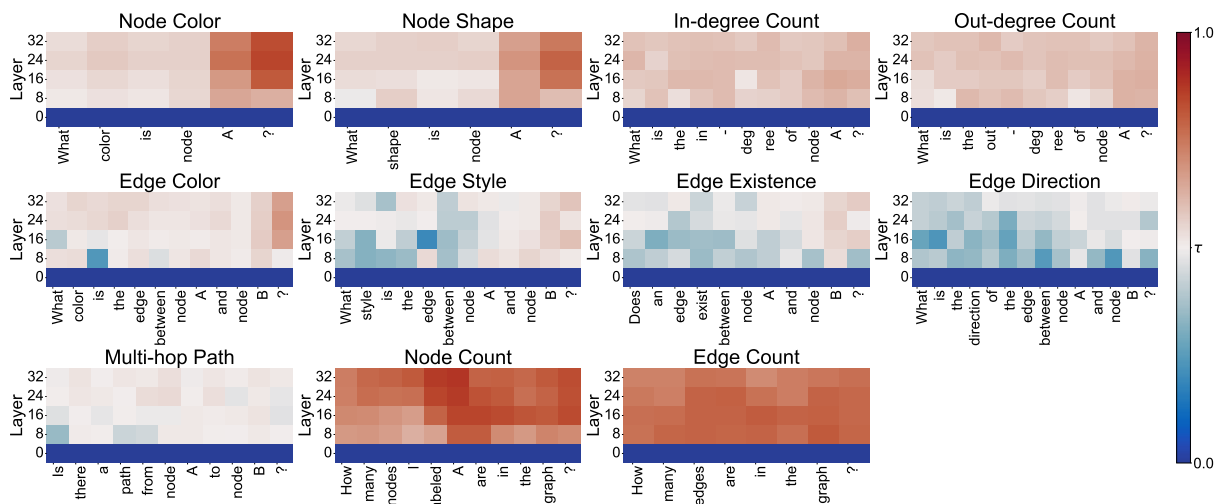


Figure 24: Probing results for text tokens in LLaVA1.5 7B. The x-axis shows token position in the question, and the y-axis shows layer position.

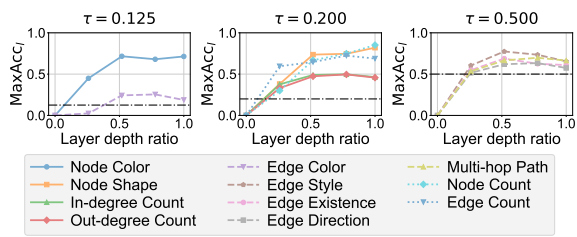


Figure 25: Layer-wise maximum accuracy in the vision encoder of Gemma3-4B-IT. The x-axis shows relative layer position (0 is the input layer, 1 is the final layer), and the y-axis shows accuracy. The black dotted line indicates the threshold.

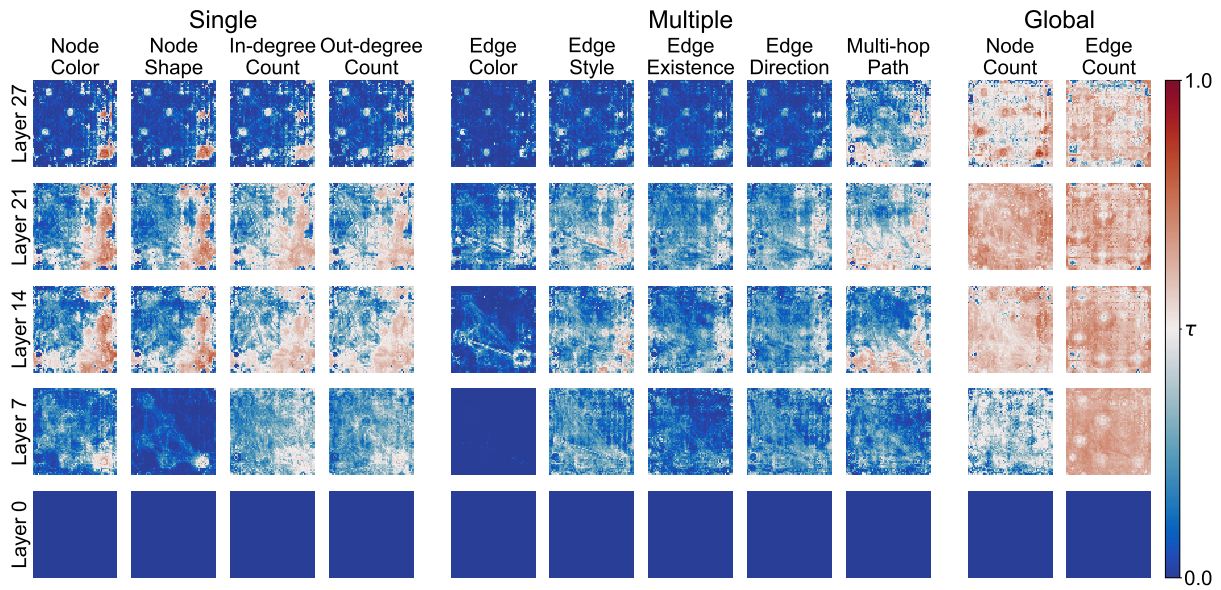


Figure 26: Accuracy for each hidden state in the image input part of the Gemma3-4B-IT vision encoder. Each heatmap shows the accuracy of individual hidden states for a specific layer and aspect.

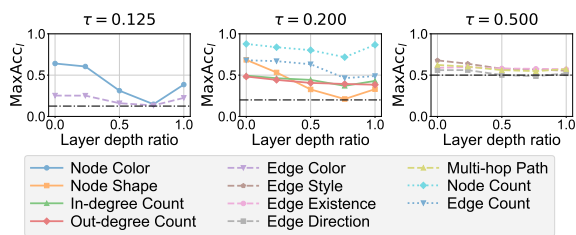


Figure 27: Layer-wise maximum accuracy in the language model of Gemma3-4B-IT. The x-axis shows relative layer position (0 is the input layer, 1 is the final layer), and the y-axis shows accuracy. The black dotted line indicates the threshold.

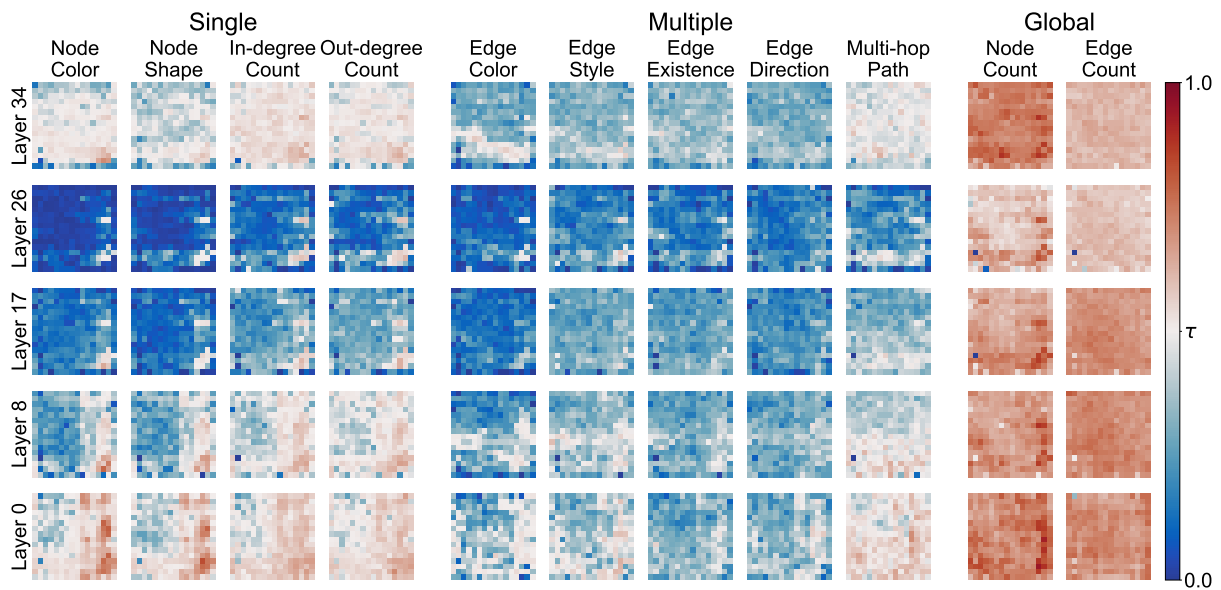


Figure 28: Accuracy for each hidden state in the image input part of the Gemma3-4B-IT language model. Each heatmap shows the accuracy of individual hidden states for a specific layer and aspect.

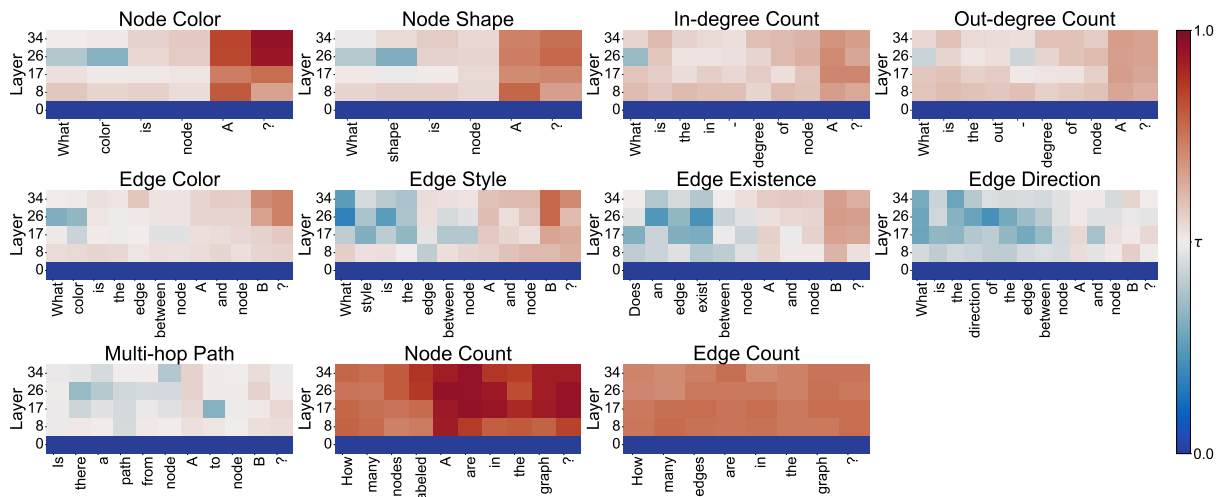


Figure 29: Probing results for text tokens in Gemma3-4B-IT. The x-axis shows token position in the question, and the y-axis shows layer position.